Improving Tiltrotor Whirl-Mode Stability with Rotor Design Variations

C. W. Acree, Jr.
NASA Ames Research Center

R. J. Peyran
U.S. Army Aeroflightdynamics Directorate

Wayne Johnson
NASA Ames Research Center

Abstract

Rotor design changes intended to improve tiltrotor whirl-flutter stability margins were analyzed. A baseline analytical model similar to the XV-15 was established, and then a thinner, composite wing was designed to be representative of a high-speed tiltrotor. While the thinner wing has lower drag, it also has lower stiffness, reducing whirl-flutter stability. The rotor blade design was modified to increase the stability speed margin for the thin-wing design. Modest amounts of blade sweep starting at 80% radius created large increases in the stability boundary. Increased control-system pitch stiffness also improved stability. Appropriate combinations of sweep and pitch stiffness completely eliminated whirl flutter within the speed range examined; alternatively, they allowed large increases in pitch-flap coupling (delta-three) for a given stability margin. A limited investigation of rotor loads in helicopter and airplane configuration showed only minor increases in loads.

Notation

CG   blade chordwise center of gravity, positive forward of EA

C_T/σ thrust coefficient, divided by solidity

EA   elastic axis

QC   blade quarter chord, positive aft of EA

R rotor radius

t/c wing thickness-to-chord ratio

Δ change in blade chordwise QC or CG position

δ_3 kinematic pitch-flap coupling ratio

μ advance ratio

1. Introduction

Coupled wing/rotor whirl-mode aeroelastic instability is the major barrier to increasing tiltrotor speeds. Increased power, thrust, and rotor efficiency are of no avail unless the whirl-mode stability boundary can be improved. With current technology, very stiff, thick wings of limited aspect ratio are essential to meet the stability requirements, which severely limits cruise efficiency and maximum speed. Larger and more efficient tiltrotors will need longer and lighter wings, for which whirl-mode flutter is a serious design issue.

This research investigated the unusually simple approach of sweeping the outboard blade sections to improve the stability boundary of the full aircraft. Initial results are given in Ref. 1. The research was extended to include variations in control system stiffness and pitch-flap coupling (δ_3).

The design and analysis of a new, reduced-thickness wing is briefly described. A CAMRAD II analytical model is described, including a matrix of parametric variations of the rotor design. The paper then discusses studies of swept blades and the effects of control-system stiffness and pitch-flap coupling. Finally, the effects on blade loads are summarized.

2. Background

The research began with a very simple, unpowered, table-top model of a wing and rotor (Fig. 1), built of balsa wood and driven as a windmill by an ordinary box fan. The wing was a ladder-frame structure with no aerodynamic shell, and the rotor was a two-bladed, teetering design. This was the simplest design possible for testing whirl flutter. The 17-in diameter rotor had an adjustable weight on a rod extending ahead of the leading edge of each tip. Adjusting the chordwise weight position produced dramatic improvements in whirl-mode stability (Ref. 2).
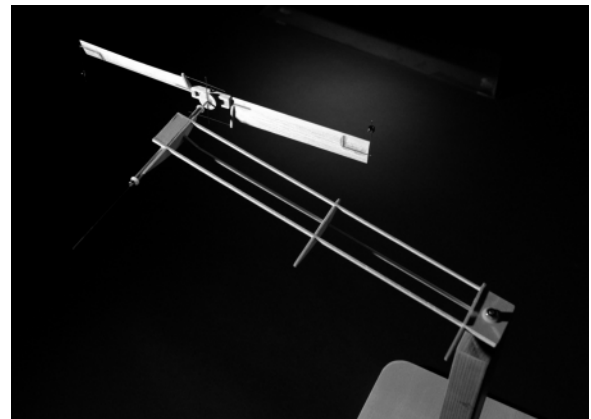
Fig. 1. Table-top tiltrotor whirl-flutter model with tip weights.

Although hardly rigorous, the results were compelling and led immediately to analyses with CAMRAD II (Ref. 3). A semi-span analytical model of the XV-15 confirmed the results of the table-top model. The analytical model and its developments reported here have roots in earlier work reported in Ref. 4.

In classic flutter theory, the distance between the center of gravity and the aerodynamic center is a key parameter. This suggested that moving the aerodynamic center aft should have similar effects to moving the center of gravity forward. The CAMRAD II model was

accordingly extended to examine an aerodynamic offset, but near the root of the blade instead of the tip. The aerodynamic offset improved whirl-mode stability, confirming the hypothesis. These favorable, preliminary results led directly to the more systematic efforts reported herein.

A major driver for the research is the desirability of thinner, more efficient wings than used on the XV-15 and V-22. Accordingly, a new, thin wing was designed to provide a more challenging stability baseline. Because the semi-span CAMRAD II model could not analyze antisymmetric wing modes, a full-span CAMRAD II model of the XV-15 was also developed.

3. Analytical Model

The new CAMRAD II model was based closely on an existing model of the XV-15, chosen because it is well-proven for stability analysis and thoroughly understood by the authors. See Refs. 4 and 5 for correlation of CAMRAD predictions with measured stability and loads.

Figure 2 is a three-view of the XV-15 with pertinent dimensional data; the moderate aspect ratio of the thick wing is clearly evident. (Detailed specifications are given in Refs. 6 and 7.) The model was altered in several ways from the original representation of the XV-15, including a different wing, a simplified drive train, and

deletion of wing aerodynamic damping. The new wing model is discussed below. The other changes were made to prevent confounding the effects of rotor parametric variations with the effects of drive-train modes and wing aerodynamic damping.

3.1 Airframe

To provide an appropriate baseline for whirl-flutter stability studies, a notional XV-15 with a thin, high-speed, graphite epoxy wing was conceptually defined. The new wing has the same planform as the original XV-15 wing, but with a thickness-to-chord ratio (t/c) of 15%, a value typical of current commuter aircraft, instead of 23%. Airframe drag was arbitrarily reduced by 25% to simulate the improved aerodynamics expected from a thinner wing and other drag improvements typical of a high-speed design. The new wing was designed strictly for strength; no allowance was made for aeroelastic stability.

The wing characteristics were estimated using the methods presented in Ref. 8. The structural concept is a constant cross-section, uniform wall thickness single-cell torque box. The torque box reacts beam bending, chord bending, shear and torsion loads. Upper and lower spar caps provide additional beam bending strength. The wing structure was sized based on static strength to meet 2-g jump take off with the nacelles positioned at 90-deg
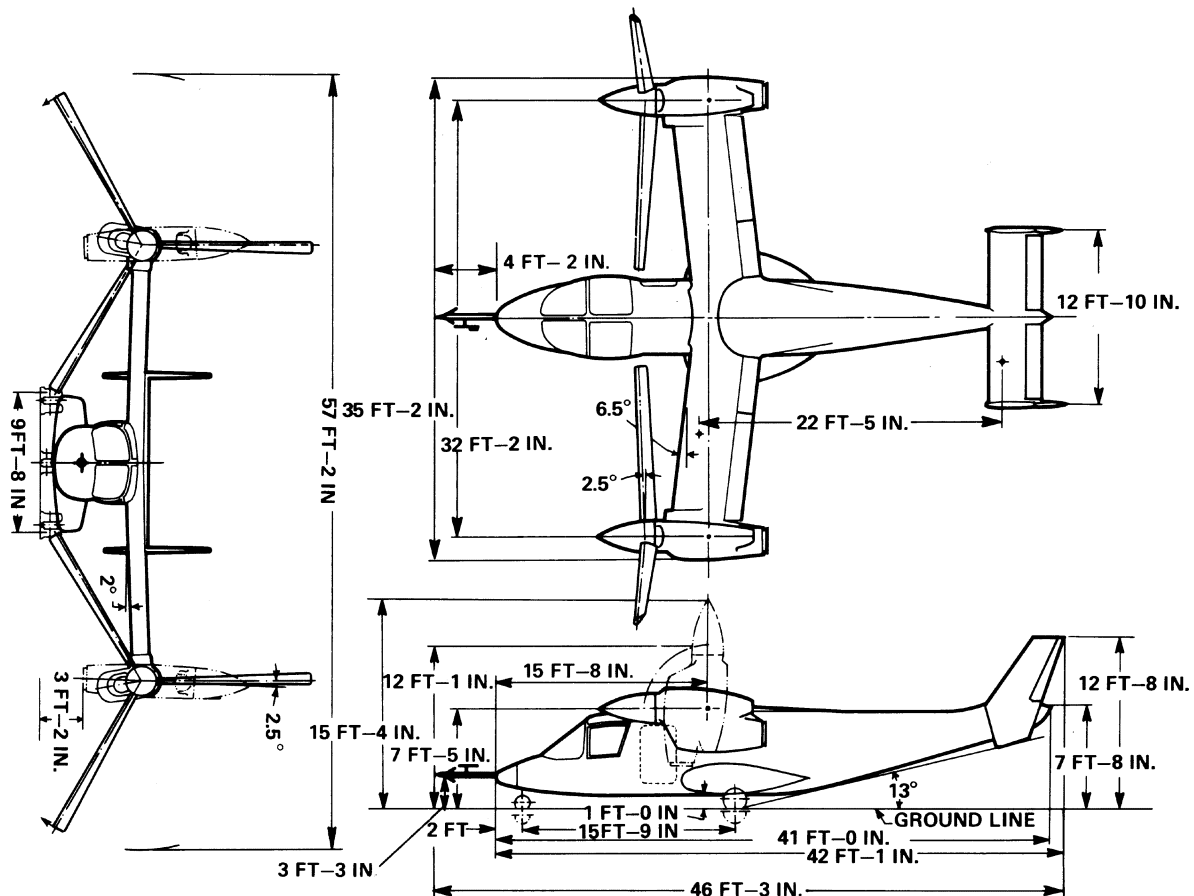
Fig. 2. XV-15 tiltrotor aircraft geometry, with 23% *t/c* wing (Ref. 6).

(helicopter mode) and 4-g pull-up with the nacelles at 0-deg (airplane mode). The wing was calculated to have a static torsional divergence speed of 529 knots at sea-level standard conditions. The design characteristics of the new wing are compared with the original XV-15 in Table 1.

Table 1. Wing structural comparison.

	XV-15 wing	Thin wing
t/c, %	23	15
Weight, lb	946	579
Material	Aluminum	Graphite epoxy
Stiffness, lb-in^2:		
Beam bending	3.70E+09	1.98E+09
Chord bending	1.12E+10	7.59E+09
Torsion	2.80E+09	1.33E+09

3.2 Finite Element XV-15 Model

To calculate aeroelastic stability, CAMRAD II couples externally generated wing modes to internally generated rotor modes. Merely lowering the wing frequencies does not result in mode shapes realistic for a thinner wing. The new wing was modeled in NASTRAN (Ref. 9) to generate modal inputs for CAMRAD II.

A structural model for the XV-15 wing (23% t/c) was developed using the XV-15 finite-element stick model by Wolkovitch et al. (Ref. 10) as a starting point. The model uses one-dimensional elements exclusively, hence the name "stick" model. This simple model is based on the XV-15 geometry (Fig. 2, Ref. 6), weights (Ref. 11), and wing structural characteristics (Ref. 12). The model consists of a 10-element elastic wing with a rigid fuselage and rigid wing-tip mounted nacelles. Two concentrated masses model the left and right rotors and hubs.

The 15% t/c wing stiffness and mass characteristics were input into the XV-15 stick model and analyzed in the same manner as for the thick wing. The aeroelastic instability speed was reduced from 335 knots (anti-symmetric beam mode) for the XV-15 with 23% t/c wing to 275 knots (antisymmetric beam mode) for the XV-15 with the conceptual 15% t/c wing. The CAMRAD II model of the XV-15 with 15% t/c wing is the baseline for evaluating proprotor design options, except where noted below.

The primary purpose of the thinner wing, at least as it applies to the present research, is to lower the whirl-mode airspeed stability boundary to better reveal the effects of parametric variations of the rotor. Because the rotor was not redesigned for higher speeds, the thin wing is of limited value for increasing cruise performance. Nevertheless, the new wing provides an adequate baseline, so the notional model was not further optimized.

3.3 Rotor

The baseline rotor used in the study was the original XV-15 steel-blade rotor, with a 2.5-deg precone titanium hub and −15-deg delta-three (nominal). This is a rigid (stiff-in-plane) rotor with a gimbaled hub. The inboard aerodynamic sections start with a 17-in chord at 12% radius, linearly tapering to a 14-in chord at 25% radius; the chord is constant from there to the tip (Fig. 3). Total effective blade twist is 45 deg over a 150-in radius (Ref. 13). The entire blade has a 1-deg aft aerodynamic sweep, with the quarter-chord line intersecting the pitch axis at 75% radius.

The rotor was modeled in CAMRAD II with a gimbal, two bending modes, one torsion mode, flexible pitch link, and rigid drive train, which is adequate for whirl-flutter analysis. The left-right symmetry of the XV-15 was exploited by calculating symmetric and anti-symmetric modes separately.

The rotor parametric variations were distributed among four radial segments, numbered 1 to 4 from root to tip as shown in Fig. 3. For simplicity, stepwise offsets were analyzed first. The aerodynamic center was offset aft in five increments of 5% of tip chord. (Local chord was not used, lest the inboard taper confound the results by creating an effective forward sweep along part of segment #1).

The aerodynamic center shifts were effected by shifting the airfoil aft with respect to the pitch axis, which in this model is the same as the blade elastic axis (EA). The airfoil was referenced to the quarter chord (QC). Figure 3 shows an example of 10% QC aft offset at the tip segment.

The center of gravity (CG) was offset forward in increments of 5% tip chord to match the magnitudes of the QC offsets. The maximum offset was therefore 25% chord, which placed the CG at the leading edge. The two types of offset were analyzed separately. There were thus five discrete values of two parameters each, at four separate radial segments, making a matrix of 40 variations in addition to the baseline.
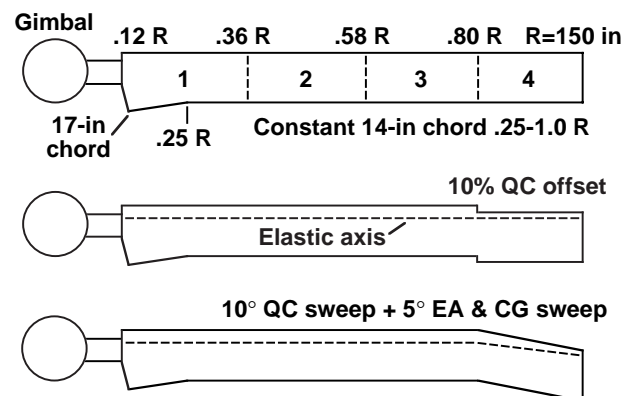
Fig. 3. XV-15 rotor blade planform (45-deg twist and 1-deg baseline sweep not shown).

The stepped modifications were not intended to represent producible rotors, but to reveal the effects of the design parameters on stability. More realistic swept-tip blades were subsequently analyzed, as discussed later in this paper.

Aerodynamic and mass offsets are conceptually similar, in that they both increase the chordwise distance between the center of gravity and aerodynamic center. This is the classic means of increasing flutter stability of an isolated airfoil. Because of the highly coupled nature of whirl-mode instability, it also increases the stability of the entire rotor-wing dynamic system. However, the effects of aerodynamic offset are much stronger than those of mass offset, as will be shown.

3.4 Trim Criteria

Limited-power trim was used to represent normal flight-test operations, wherein the aircraft is trimmed to level flight up to the power- or torque-limited airspeed, then allowed to descend as necessary to achieve the desired airspeed at the torque limit. Here a torque limit of 130,000 in-lb was used, reached at 275 knots with the thin wing. Zero power (windmill state) is a possible emergency flight condition (engine out), so it was also checked. For this research, limited-power trim always had a lower instability airspeed than zero power, although not by a large margin. Results for only the former are reported herein.

The rotor was trimmed to 458 rpm (76% of hover design rpm), at sea-level standard conditions. This is the original design cruise rotor speed and not representative of current XV-15 operations; it was chosen because it is a nominal design point and highlights the effects of the parametric variations. The speed range was 150 to 400 knots true airspeed, with trim and stability calculated in 25-knot increments.

4. Stability Predictions

Adding up the cases discussed above, there are 11 airspeeds for both trim criteria (zero power and limited power), applied to each of the 40 parametric variations, plus the thick- and thin-wing XV-15 models with the unmodified rotor, for a total of 924 cases. It is practical to present only a general overall summary for the stepped-offset designs.

4.1 Baseline Checks

Figures 4 and 5 compare the CAMRAD II predictions for thick- and thin-wing XV-15 whirl modes, plotted as damping versus airspeed for each of the wing modes. The intersections of the individual damping curves with the zero-damping axis define the stability boundaries for each mode; the overall whirl-flutter boundary is of course that of the least stable mode.

There are six wing modes to be examined: beamwise bending, chordwise bending, and torsion, each in symmetric (Fig. 4) and antisymmetric (Fig. 5) forms. The
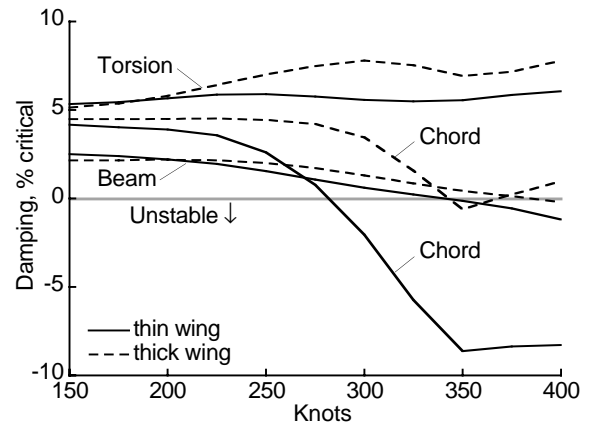
Fig. 4. Symmetric whirl-mode damping versus airspeed for the thick- and thin-wing models.
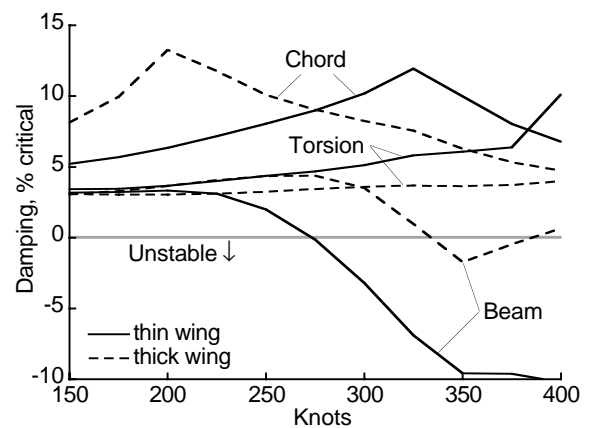
Fig. 5. Antisymmetric whirl-mode damping versus airspeed for the thick- and thin-wing models.

mode labels are somewhat arbitrary because the mode shapes rarely show pure bending, torsion, or chordwise deflections. This is especially true for the antisymmetric chord and torsion modes. Moreover, the blade collective lag mode couples strongly with the wing modes at high speeds.

At 400 knots, the tip Mach number is 0.82, placing the tip airfoil section inside the transonic regime. The blade section lift curve slope is decreasing at that point, which improves stability. This effect can be clearly seen in several of the modes, most notably symmetric chord (Fig. 4) and antisymmetric beam and torsion (Fig. 5).

4.2 Summary of Parametric Variations for Stepped Offsets

Figures 6 and 7 summarize the changes to the overall stability boundary caused by the variations in blade QC and CG, modeled as stepped offsets. For the analyses discussed in this section, only one type of offset was applied at a time, and at only one radial segment at a time. The thin-wing airframe model was used in all stepped-offset cases.
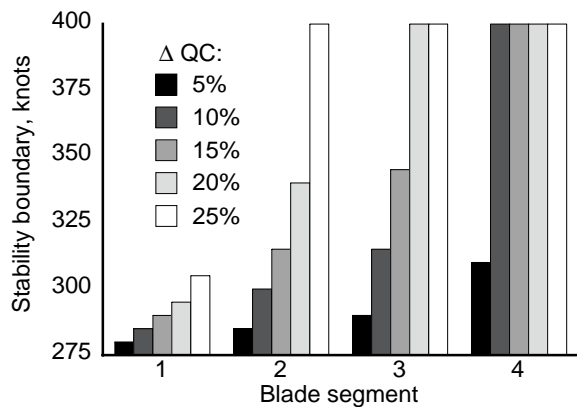
Fig. 6. Whirl-mode stability boundaries for quarter-chord offsets, thin-wing model.
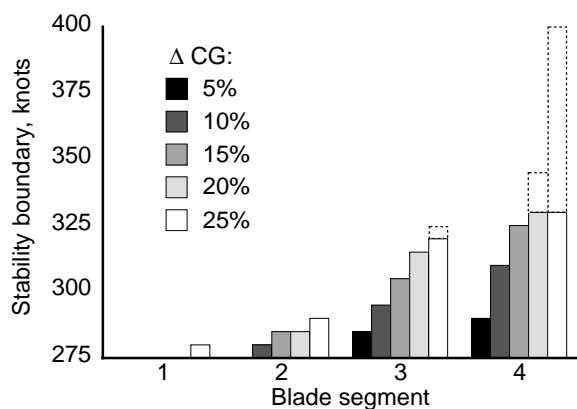
Fig. 7. Whirl-mode stability boundaries for center-of-gravity offsets, thin-wing model. Dotted bars are antisymmetric mode limits.

The limiting airspeed was interpolated to the nearest 5 knots for each value of offset in Figs. 6 and 7. The lower limit of each plot is 275 knots, the stability boundary for the thin-wing model with the unmodified rotor. The stability boundary of the modified rotor never dropped below this speed. The upper limit of 400 knots is the maximum speed analyzed.

Eleven of the 40 QC and CG variations increased the instability airspeed by 60 knots or more, which at a minimum fully recovered the stability boundary of the original, thick-wing XV-15 model.

It is immediately apparent that QC offsets are much more effective than CG offsets: usually at least twice as much so (compare Fig. 6 to Fig. 7). Offsets at the tip are more effective than at the root for both types of offset.

For QC offsets, the limiting mode was usually antisymmetric beam, except for the 10% aft QC offset at segment #2, for which the symmetric beam mode determined the instability airspeed.

For CG offsets, the limiting mode was also usually the antisymmetric beam mode. The three exceptions were 25% forward CG offset at segments #3 and #4, and 20%

forward CG offset at segment #4, for which the symmetric beam mode was the limiting mode.

The dotted lines in Fig. 7 represent the stability boundaries of the antisymmetric beam mode. Aerodynamic damping was neglected in the stability analyses. It would have increased the damping of the symmetric beam mode more than the other modes, so that all values would have shifted upwards, but by unequal amounts. The stability trends would then more closely follow the dotted bars in Fig. 7.

The extended stability boundaries for segment #4 in Fig. 7 are generally similar to the boundaries of segment #2 in Fig. 6, which reveals that both types of offset have similar effects on stability, aside from the greater overall effectiveness of QC offsets.

The effects of QC offsets were more pronounced than expected. The 400-knot limit of this study prevented a complete evaluation of the ultimate effectiveness of QC offsets at very high speeds, but exploitation of large stability improvements would require a reoptimized rotor. A 400-knot-class proprotor would have different airfoils, twist and planform, and would therefore be expected to show different sensitivities to the parametric variations considered here.

4.3 Swept-Tip Blades

Figures 6 and 7 together imply that swept tips would increase whirl-mode stability. Aft sweep would move the CG in an unfavorable direction, but the greater sensitivity of damping to QC offset would cause a net increase in stability. Sweep would also maximize the amount of offset at the tip for a slight improvement over a stepped offset, and would make for more practical blade construction.

Figure 3 shows an example blade with a swept tip. It has 10-deg sweep over the outer 20% radius, the maximum analyzed in this study; this approximates the best of the stepped-offset designs and is of course far more practical. Two variations were analyzed: a conventional swept tip with equal aerodynamic and structural sweep, and a tip with its elastic axis and center of gravity swept one-half as much as the quarter chord. The latter design would be feasible as long as the sweep did not start too far inboard.

Figures 8 and 9 show the variation in damping with sweep for blades with conventional sweep (Fig. 8) and with structural sweep of one-half the aerodynamic sweep (Fig. 9). In Fig. 9, the damping of the least stable modes is much improved over that of Fig. 8; at high values of sweep, it is fully stable.

It should be emphasized that all analyses reported here are based on the original XV-15 steel blades, for which the manufacturability of any modification is highly problematical. A swept tip would be much easier to implement with a modern, composite structure. Because the particular designs considered here have no likelihood
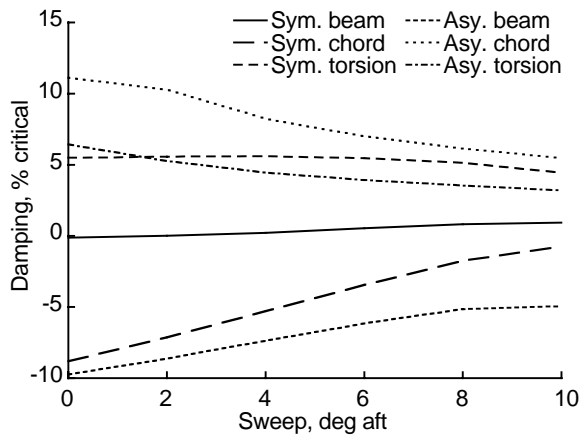
Fig. 8. Variation of damping with conventional sweep at 350 knots.
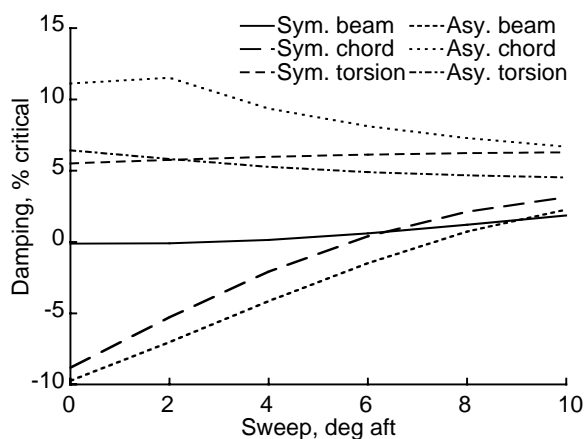
Fig. 9. Variation of damping with sweep at 350 knots; the structural sweep is one-half the aerodynamic sweep.

of being constructed, and because the results shown in Fig. 9 are more than adequate to illustrate the benefits of the concept, no further optimization of the blade design was undertaken. A blade with 10-deg aerodynamic and 5-deg structural sweep was chosen for further study, as discussed in the following sections.

4.4 Control-System Stiffness

The stiffness of the control system is predicted to have a strong effect on aeroelastic stability, as shown in Fig. 10 for the baseline rotor. The baseline pitch stiffness seen by the blade is multiplied by a stiffness factor, against which damping is plotted. (The baseline value is 22,400 ft-lb/rad.) CAMRAD II allows the pitch links to be analytically locked, yielding the equivalent of infinite stiffness. Infinite stiffness yields damping values negligibly different from a stiffness factor of 100, so the stiffness scale in Fig. 10 is truncated at that value. For clarity, the scale is logarithmic to expand the damping curves at low values of stiffness while simultaneously revealing the asymptotic behavior at high values. Damping was calculated at 350 knots for the thin wing, consistent with Figs. 8 and 9.
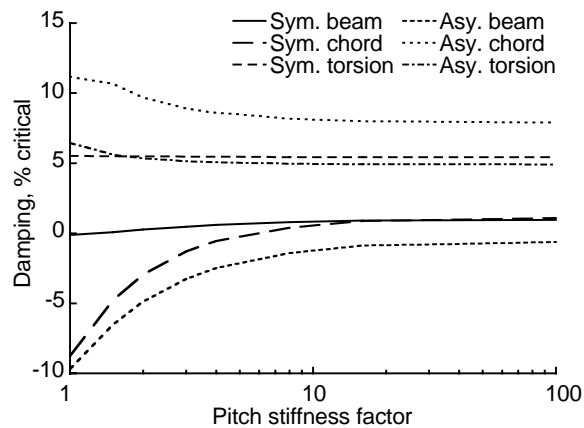
Fig. 10. Variation in damping with pitch stiffness factor for the baseline XV-15 rotor at 350 knots.

Figure 10 shows that about half of the maximum increase in damping is obtained with a pitch stiffness factor of two, and further increases in stiffness yield progressively diminishing increases in damping. A stiffness factor of two was used in selected analyses below. No further optimization was undertaken, largely because of the diminishing effectiveness of greater stiffness. The V-22 has roughly three times the scaled pitch stiffness of the XV-15, so a stiffness factor of two is reasonable.

Figure 11 shows the results of combining tip sweep with an increased control-system stiffness. As in Figs. 8 and 9, the aerodynamic sweep was twice the structural sweep. The asymptotic behavior of damping with sweep reduces the effect of increasing sweep (compare Fig. 11 with Fig. 8); at high enough values of sweep, the increase in damping with sweep is negligible. However, the system becomes stable at a lower value of sweep: about 7 deg instead of 9 deg, a useful improvement.

The trends of damping with airspeed are shown in Fig. 12 for combined tip sweep and increased control-system stiffness. The rotor is the same as that analyzed for Fig.
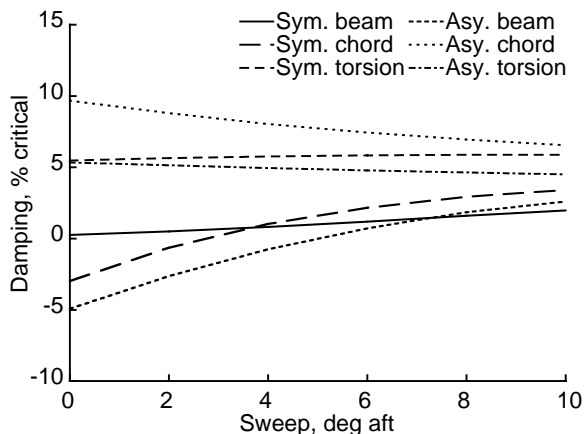
Fig. 11. Variation of damping with sweep at twice the baseline pitch stiffness at 350 knots; the structural sweep is one-half the aerodynamic sweep.

11 at maximum sweep. For ease of comparison, the format is the same as Figs. 4 and 5; the "reference rotor" lines below correspond to the "thin wing" lines in Figs. 4 and 5. Note that all whirl modes, including the symmetric beam mode, show little variation in damping with airspeed; the wing/rotor system is now completely stable.
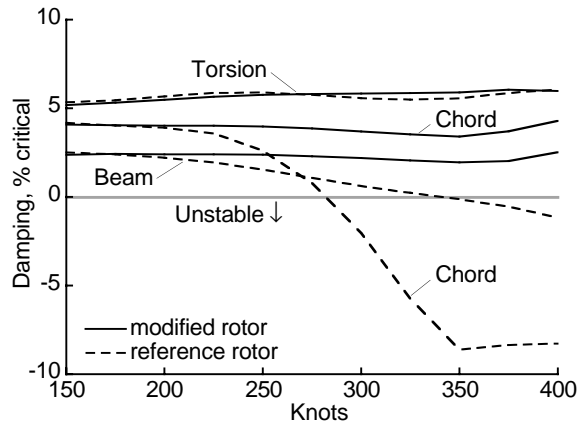
Fig. 12a. Symmetric whirl-mode damping at twice the baseline pitch stiffness, 10-deg aerodynamic sweep and 5-deg structural sweep.
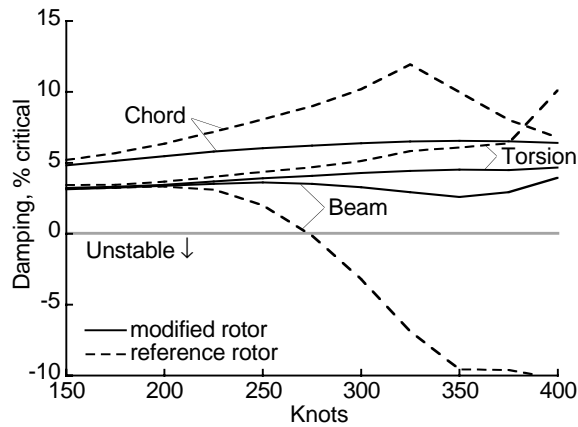
Fig. 12b. Antisymmetric whirl-mode damping at twice the baseline pitch stiffness, 10-deg aerodynamic sweep and 5-deg structural sweep.

4.3 Delta-three variations

So far in this paper, blade modifications have been studied for the purpose of extending the XV-15 whirl-flutter boundary for a thin wing. Improvements to whirl-mode damping can be exploited for other purposes, an example of which is discussed in the following paragraphs.

Delta-three (δ_3) is the kinematic coupling between blade flapping and pitch (Ref. 14). As defined herein, positive δ_3 causes nose-down pitching for upwards blade flapping. This counterintuitively *decreases* stability for some blade modes, typically lag modes. The realization that negative δ_3 is stabilizing was a major conceptual breakthrough necessary for the successful development of the XV-15 (Refs. 7 and 15).

Because the effective flapping hinge is at the center of rotation of a gimbaled rotor, a literal skewed hinge is not possible on the XV-15, so offset pitch horns must be used. The XV-15 has trailing pitch horns, as shown in Fig. 13. Furthermore, it is extremely difficult to arrange the pitch horns to achieve small values of δ_3 without mechanical interference, especially for rotors with four or more blades. As the magnitude of δ_3 increases, whirl-mode stability rapidly decreases.
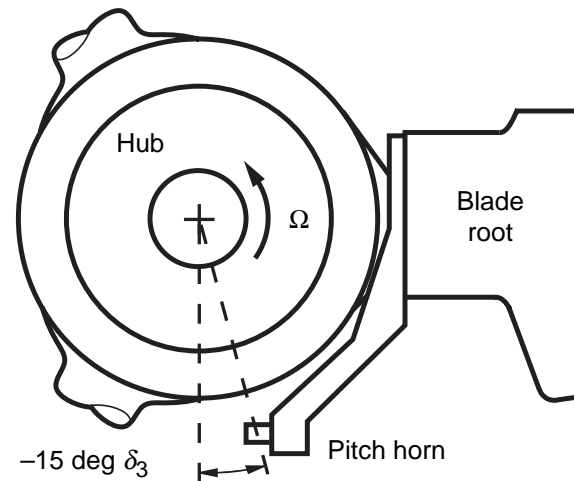
Fig. 13. XV-15 hub and trailing pitch horn.

These effects constrain practical design values of δ_3 to a narrow range of negative values. The XV-15 design value of δ_3 is –15 deg (Ref. 6), realized by a trailing, offset pitch horn. All values of δ_3 discussed herein are nominal values; the actual value varies as the pitch horn moves with changing collective and cyclic control inputs.

Figure 14 shows the variation of damping with δ_3 for the baseline XV-15 (thick wing) and unmodified rotor. The airspeed is 300 knots, the design maximum. The damping predicted by CAMRAD II becomes negative between –20- and –25-deg δ_3. The actual aircraft must have a margin of stability, so the design magnitude of δ_3 must be less than the zero-damping value. Figure 14 indicates that –15 deg is a reasonable value, which is consistent with XV-15 experience.

Damping of the unstable modes varies almost linearly with δ_3 until it approaches the limiting, stable value consistent with Figs. 8-11 (although maximum anti-symmetric beam damping is a bit higher). Damping for positive δ_3 is not shown because certain rotor modes, principally blade lag modes coupled with wing modes, are always unstable.

Figure 15 shows results for a rotor with 10-deg aero-dynamic sweep and 5-deg structural sweep over the outmost 20% blade radius. This is the most extreme sweep plotted in Fig. 9 and is the most effective of the practical blade designs examined here. The airspeed is 300 knots, the same as Fig. 14. The δ_3 value for neutral

stability is extended to almost –45 deg. The two least stable modes at –45-deg δ_3 become the most stable modes near –35 deg, then asymptotically approach the limiting values seen in the previous plots.

The final analysis shown here combined the increased control-system stiffness with the swept tip, as in Fig. 12; the results are shown in Fig. 16. Whirl-mode damping is positive for –45-deg δ_3. This value of δ_3 was the maximum studied because no further increase is necessary for a four-bladed rotor, and because the incremental improvement caused by the increased control-system stiffness is very minor compared to Fig. 15.

5. Loads Implications

Two designs were analyzed further to estimate their effects on rotor loads. Both designs used the most effective rotors developed during this study, with 10-deg aerodynamic sweep, 5-deg structural sweep, and twice the baseline control stiffness. Design A had the 15% t/c wing with –15-deg δ_3, and Design B had the 23% t/c wing with –45-deg δ_3. These correspond to the designs analyzed for Figs. 12 and 16, respectively. Two flight conditions were analyzed:

1. Airplane mode at 250 knots, 458 rpm ($\mu = 0.70$), rotor $C_T/\sigma = 0.027$.
2. Helicopter mode (nacelle angle = 75 deg) at 80 knots, 565 rpm ($\mu = 0.18$), rotor $C_T/\sigma = 0.088$.

The airplane mode condition was chosen to ensure that the loads were calculated within the thin-wing stability boundary (Figs. 4 and 5) to provide a valid baseline reference.

Predictions of mean and 1/2 peak-to-peak oscillatory loads are plotted in Figs. 17 and 18. The figures include flap and lag bending moments at 0.35 R and pitch link force, all normalized to the reference (unmodified) rotor for the appropriate wing. Helicopter-mode loads are normalized to the helicopter reference, and airplane-mode loads are normalized to the airplane reference. Mean and oscillatory loads are plotted separately. The results for the example rotors are plotted adjacent to each other for comparison, and airplane-mode results are plotted adjacent to helicopter-mode results for each type of load (lag, flap, and pitch-link loads).

All loads analyses included six harmonics of blade motion and 12 blade modes. In airplane mode, the analysis included wing/body interference velocities at the rotor. Uniform inflow was assumed because the differences caused by blade dynamics are of interest, for which momentum theory is adequate, especially in airplane mode. Development of a full wake model for helicopter flight was not justified at this stage of the research, which is focused on flutter, not loads. The objective of the loads analysis was to check for large adverse load variations.
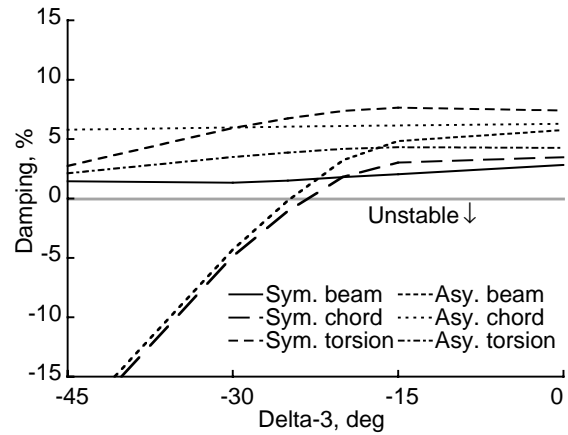
Fig. 14. Variation of damping with δ_3 for the baseline XV-15 (thick wing) and unmodified rotor at 300 knots.
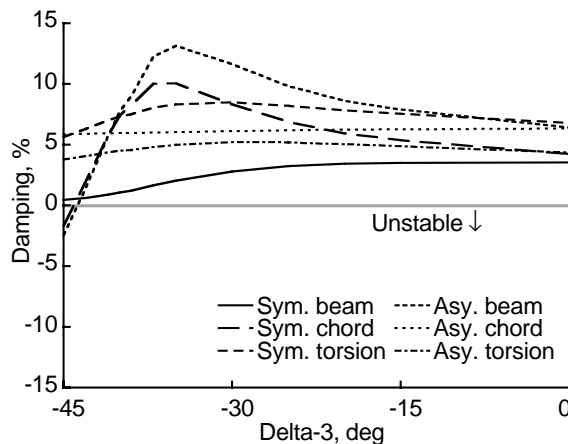
Fig. 15. Variation of damping with δ_3 for the baseline XV-15 with swept tips at 300 knots.
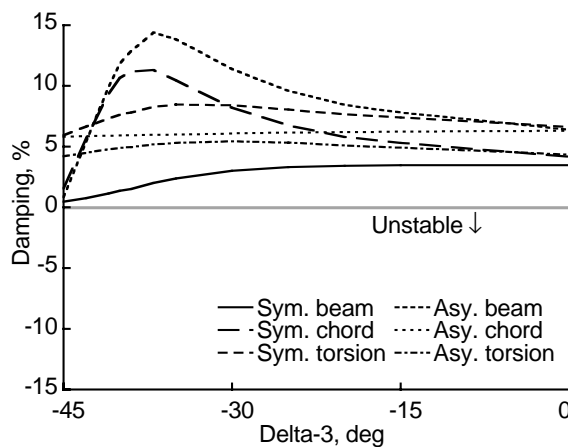
Fig. 16. Variation of damping with δ_3 for the baseline XV-15 with swept tips and twice the baseline pitch stiffness at 300 knots.

Examination of Fig. 17 shows that none of the design variations had severely adverse effects on mean loads in airplane mode. Mean lag-bending loads were always reduced compared to the baseline rotor.

In Fig. 18, lag- and flap-bending oscillatory loads were little affected, but pitch-link loads were increased for both designs. However, the normalization against loads in the same flight condition exaggerates the effect. In fact, oscillatory pitch-link loads were much lower in airplane mode than in helicopter mode.
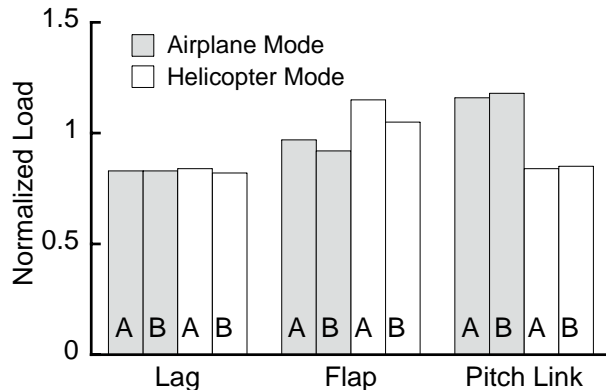
Fig. 17. Mean rotor loads, normalized to the baseline rotor, for rotor designs A and B.
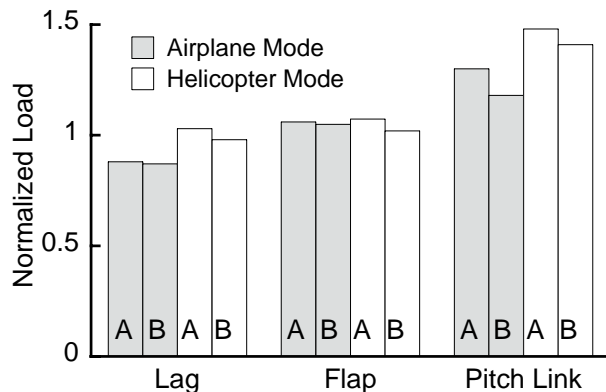
Fig. 18. Oscillatory rotor loads, normalized to the baseline rotor, for rotor designs A and B.

Although not a comprehensive loads survey, these results are enough to show that loads increases should be acceptable, especially for the swept-tip design. Furthermore, no attempt was made to adjust balance weights or otherwise tune the rotor for loads, so it should be possible to reduce the loads below those shown here. The key result is that there exist combinations of parameters that give large increases in the whirl-mode stability boundary without excessive increases in loads.

6. Conclusions

The XV-15 rotor was analyzed with CAMRAD II to examine the effects on whirl-mode aeroelastic stability of chordwise offsets of the rotor blade quarter chord and center of gravity relative to the elastic axis. The XV-15 model was modified to have a thinner wing (15% *t/c*) to

better reveal the effects of the blade modifications. Small rearward offsets of the quarter-chord created large increases in the stability boundary; the effect was strongest for offsets at the tip. Forward offsets of the blade center of gravity had similar effects, but reduced in magnitude.

Swept-tip blades showed stability improvements similar to stepped-offset designs, as expected. When combined with increased control-system stiffness, the swept-tip blades completely eliminated whirl-mode flutter for the thin wing within the range of airspeeds analyzed (up to 400 knots). For the baseline XV-15 at 300 knots, the swept tips allowed δ_3 (pitch-flap coupling) to be increased to –45 deg without whirl flutter. Blade loads remained acceptable.

These results can be applied to tiltrotors in several ways, most obviously to reduce the wing thickness for improved cruise performance while retaining adequate whirl-mode stability margins. In the present study, the wing thickness-to-chord ratio was reduced from 23% to 15% without decreasing the whirl-mode boundary. Thickness could in principle be retained while reducing weight or increasing aspect ratio, as appropriate for the performance goals of a particular design.

Offsets of the blade aerodynamic center and center of gravity, or the equivalent sweep, may be treated as primary design variables because of their powerful effects on whirl-mode stability. Control-system stiffness should also be considered a design variable for stability.

The improvements to whirl-mode stability can be used to expand the range of δ_3. A sufficiently large increase in δ_3 would permit building four-bladed rotors with otherwise conventional gimbaled hubs.

Follow-on research could usefully examine the effects for a rotor explicitly designed for very high speeds, with re-optimized twist, airfoil sections, taper, etc. The analysis could be extended to more radical blade concepts, such as inverse-taper and external mass booms, and to further examine the interplay between blade design parameters and control system stiffness, δ_3, and other variables. These concepts will eventually require validation with wind-tunnel and flight tests.

7. Acknowledgments

8. References

1. Acree, C. W., Peyran, R. J., and Johnson, W. "Rotor Design for Whirl Flutter: An Examination of Options for Improving Tiltrotor Aeroelastic Stability Margins,"

American Helicopter Society 55th Annual Forum, Montréal, Quebec, Canada, May 25-27, 1999.

2. Madden, J. F., III, and Peyran, R. J., "Aeroelastic Stability Enhancer for Tilt-Rotor Aircraft," Invention Disclosure, NASA Case No. ARC-14298-1CU, May 1998.

3. Johnson, W., "CAMRAD II Comprehensive Analytical Model of Rotorcraft Aerodynamics and Dynamics — Theory Manual," Johnson Aeronautics, Palo Alto, California, 1993.

4. Johnson, W., Lau, B. H., and Bowles, J. V., "Calculated Performance, Stability, and Maneuverability of High Speed Tilting Proprotor Aircraft," Twelth European Rotorcraft Forum, Garmisch-Partenkirchen, Federal Republic of Germany, September 22-25, 1986.

5. Johnson, W., "CAMRAD II Comprehensive Analytical Model of Rotorcraft Aerodynamics and Dynamics — Rotorcraft Applications," Johnson Aeronautics, Palo Alto, California, 1993.

6. Maisel, M., "Tilt Rotor Research Aircraft Familiarization Document," NASA TN X-62, 407, January 1975.

7. Maisel, M., Giulianetti, D. J., and Dugan, D. C., *The History of the XV-15 Tilt Rotor Research Aircraft,* NASA SP-2000-4517.

8. Chappell, D. P., and Peyran, R. J., "Methodology for Estimating Wing Weights for Conceptual Tilt Rotor and Tilt Wing Aircraft," Society of Allied Weight Engineers 51st Annual Conference, Hartford, Connecticut, May 1992.

9. MacNeal-Schwendler Corporation, "MSC NASTRAN for Windows — Evaluation Guide and User's Manual," MSC Inc., Los Angeles, California, 1997.

10. Wolkovitch, J., Wainfan, B., Ben-Harush, Y., and Johnson, W., "Application of the Joined Wing to Tiltrotor Aircraft," NASA CR-177543, November 1989.

11. Arrington, W., Kumpel, M., Marr, R., and McEntire, K., "XV-15 Tilt Rotor Research Aircraft Flight Test Data Report," NASA CR-177406, June 1985.

12. Staff of Bell Helicopter Company, "V/STOL Tilt Rotor Research Aircraft — Volume 3: Structural Loads and Dynamics," Bell Helicopter Co. Report No. 301-199-003, 1974.

13. Staff of Bell Helicopter Company, "Advancement of Proprotor Technology. Task II — Wind-Tunnel Test Results." Bell Helicopter Company Report 300-099-004, NASA CR-114363, September 1971.

14. Johnson, W., *Helicopter Theory*, Princeton University Press, 1980.

15. Gaffey, T. M., "The Effect of Positive Pitch-Flap Coupling (Negative δ_3) on Rotor Blade Motion Stability and Flapping," *Journal of the American Helicopter Society*, Vol. 14, No. 2, April 1969.